Optical high resolution cross section imaging of a human breast model using independent component analysis

M. Xu[a], M. Alrubaiee[b], S. K. Gayen[b], H. Savage[c], and R. R. Alfano[b]

[a]Department of Physics, Fairfield University, Connecticut, CT 06824
[b]Institute for Ultrafast Spectroscopy and Lasers and Department of Physics,
The City College and Graduate Center of City University of New York, New York, NY 10031
[c]Department of Otolaryngology, New York Eye and Ear Infirmary, New York, NY 10003
Email: mxu@mail.fairfield.edu

ABSTRACT

Optical imaging using independent component analysis (OPTICA) is enhanced to provide a high resolution cross section imaging of objects in a turbid medium by a backprojection technique. The performance is demonstrated by imaging a human breast model made of *ex vivo* human breast tissues. Cancerous site of 5mm size is detected at the midplane of the 33mm thick breast model. The reconstructed cross section image compares favorably with pathology findings.

Keywords: optical imaging, independent component analysis, cross section, human breast

1. INTRODUCTION

Biomedical diffuse optical tomography (DOT) has received significant attention and development in the past two decades and has been applied to image, such as, human breast, infant brain and joints. The state of art diffuse optical tomography currently relies on an iterative image reconstruction approach to construct the optical properties of the interior of the medium. This approach is computationally demanding yet provides limited spatial resolution. [1] Reconstruction of images with adequate spatial resolution and accurate localization and characterization of the inhomogeneities remain a formidable task.

An alternative optical imaging approach is optical imaging using independent component analysis (OPTICA). The principle of OPTICA is to first sort out the signal due to individual inhomogeneity and then perform three dimensional (3D) localization and characterization for each inhomogeneity, using a massive data set generated by a multi-source illumination and multi-detector signal acquisition scheme. Independent component analysis has been extensively applied in fields such as Electroencephalogram (EEG) and functional MRI (fMRI) and shown effective in separating signals from different brain activity centers. Our previous work has shown that such an approach significantly improves the sensitivity to small/weak absorptive, scattering and/or fluorescence inhomogeneities and can achieve a 3D localization of the target with error less than 1mm.

In this paper, we report on a back projection method to obtain high-resolution cross-section images of targets inside highly scattering media, enhancing OPTICA. We demonstrate the performance of OPTICA by imaging a $42 \times 30 \times 33\mathrm{mm}^3$ model human breast assembled using *ex vivo* breast tissues. A $5 \times 5 \times 3\mathrm{mm}^3$ tumor was placed at the midplane. OPTICA located the tumor within $\sim 1\mathrm{mm}$ of its known position. It also identified a $10\mathrm{mm}$ low scattering structure at midplane, and a $3\mathrm{mm}$ low scattering structure near the surface. Subsequent pathological analysis confirmed the tumor, and identified the other two structures as glandular breast tissues. The reconstructed cross section images and optical properties of the targets were consistent with pathology findings.

Optical Tomography and Spectroscopy of Tissue VII
edited by Britton Chance, Robert R. Alfano, Bruce Jason Tromberg, Mamoru Tamura, Eva Marie Sevick-Muraca
Proc. of SPIE Vol. 6434, 643416, (2007) · 1605-7422/07/$18 · doi: 10.1117/12.703574

2. THEORETICAL FORMALISM OF OPTICAL IMAGING USING INDEPENDENT COMPONENT ANALYSIS

The presence of optical inhomogeneities inside a turbid medium perturbs the intensity of emergent light from the medium under illumination by a probing beam. In the diffusion approximation, the change of the light intensity on the boundary of the specimen due to absorptive and scattering objects (inhomogeneities) can be written as: [2, 3]

$$-\Delta I(\mathbf{r}_d, \mathbf{r}_s) = \int d^3\mathbf{r}\delta\mu_a(\mathbf{r})cG(\mathbf{r}_d, \mathbf{r})G(\mathbf{r}, \mathbf{r}_s) + \int d^3\mathbf{r}\delta D(\mathbf{r})c\nabla_{\mathbf{r}}G(\mathbf{r}_d, \mathbf{r}) \cdot \nabla_{\mathbf{r}}G(\mathbf{r}, \mathbf{r}_s) \quad (1)$$

to the first order of Born approximation [4] when illuminated by a point source of unit power, where $\mathbf{r}_s$ and $\mathbf{r}_d$ are the positions of the probing source and the light detector on the boundary, $\delta\mu_a(\mathbf{r}) = \mu_a(\mathbf{r}) - \mu_{a_0}$ and $\delta D(\mathbf{r}) = D(\mathbf{r}) - D_0$ are the differences in absorption coefficient and diffusion coefficient, respectively, between the inhomogeneity at $\mathbf{r}$ and the background, c is the speed of light in the medium, and $G(\mathbf{r}, \mathbf{r}')$ is the Green's function describing light propagation from $\mathbf{r}'$ to $\mathbf{r}$ inside the background turbid medium of absorption and diffusion coefficients μ_{a_0} and D_0.

OPTICA assumes each inhomogeneity within the scattering medium to be a virtual source and express the change of the light intensity on the boundary of the specimen as:

$$-\Delta I(\mathbf{r}_d, \mathbf{r}_s) = \sum_j a_j(\mathbf{r}_d)s_j(\mathbf{r}_s) \quad (2)$$

where $s_j(\mathbf{r}_s)$ represents the j-th inhomogeneity illuminated by the incident wave at $\mathbf{r}_s$, and $a_j(\mathbf{r}_d)$ is the weighting matrix describing the propagation of light from the j-th inhomogeneity to the detector at $\mathbf{r}_d$. Each absorptive inhomogeneity contributes one term in Eq. (2) and each scattering inhomogeneity contributes three terms in Eq. (2). The detected change of the light intensity (2) is hence a linear mixture of signals where a_j and s_j can now be interpreted as the *j*-th weighting matrix and virtual source, respectively. Owing to the statistical independence between these virtual sources, independent component analysis of $-\Delta I$ will yield a list of independent components and recover both a_j and s_j. The number of the leading independent components gives the number of objects. The location and characterization of the *j*-th target is obtained from the analysis of the retrieved independent component (s_j and a_j) which relates directly to the source-to-object and object-to-detector Green's functions $G(\mathbf{r}_j, \mathbf{r}_s)$ and $G(\mathbf{r}_d, \mathbf{r}_j)$ and the optical property of the target where $\mathbf{r}_j$ is the position of the j-th object. [5–8]

For a slab geometry investigated here, there are three virtual sources of specific patterns (one centrosymmetric and two dumbbell-shaped) associated with one scattering inhomogeneity, whereas only one centrosymmetric virtual source is associated with one absorptive inhomogeneity. Among the three virtual sources associated with one scattering inhomogeneity, the centrosymmetric virtual source is the easiest to detect. The centrosymmetric virtual source and the corresponding weighting matrix are $s_j \propto G(\mathbf{r}_j, \mathbf{r}_s)$ and $a_j \propto G(\mathbf{r}_d, \mathbf{r}_j)$, and $s_j \propto \frac{\partial G}{\partial z}(\mathbf{r}_j, \mathbf{r}_s)$ and $a_j \propto \frac{\partial G}{\partial z}(\mathbf{r}_d, \mathbf{r}_j)$, respectively, for absorptive and scattering inhomogeneities. A simple least square fitting of the centrosymmetric component, such as

$$\min_{\mathbf{r}_j, \alpha_j, \beta_j} \left\{ \sum_{\mathbf{r}_s} \left[\alpha_j^{-1} s_j(\mathbf{r}_s) - G(\mathbf{r}_j, \mathbf{r}_s)\right]^2 + \sum_{\mathbf{r}_d} \left[\beta_j^{-1} a_j(\mathbf{r}_d) - G(\mathbf{r}_d, \mathbf{r}_j)\right]^2 \right\}. \quad (3)$$

for the absorptive object, can be used to yield the 3D location $\mathbf{r}_j$ and the strength $\alpha_j\beta_j$ of the target. When a prior knowledge about the property of the target is not available, Eq. (3) can still be used to estimate the 3D location of the target regardless absorption or scattering property of the target since $\frac{\partial G}{\partial z}(\mathbf{r}_j, \mathbf{r}_s) \simeq -\kappa G(\mathbf{r}_j, \mathbf{r}_s)$ and $\frac{\partial G}{\partial z}(\mathbf{r}_d, \mathbf{r}_j) \simeq -\kappa G(\mathbf{r}_d, \mathbf{r}_j)$ where $\kappa = \sqrt{(\mu_{a_0} - i\omega/c)/D_0}$ chosen to have a nonnegative real part with ω the modulation frequency of the incident wave.

The signal of the *j*-th target is simply given by $-\Delta I_j = a_j(\mathbf{r}_d)s_j(\mathbf{r}_s)$. On the other hand, the centrosymmetric signal of the *j*-th target can be approximately expressed as a double convolution in the form of

$$-\Delta I_j(\mathbf{r}_d, \mathbf{r}_s) = \int G(\boldsymbol{\rho}_d - \boldsymbol{\rho}, z_d, z_j)X_j(\boldsymbol{\rho})G(\boldsymbol{\rho} - \boldsymbol{\rho}_s, z_j, z_s)d\boldsymbol{\rho} \quad (4)$$

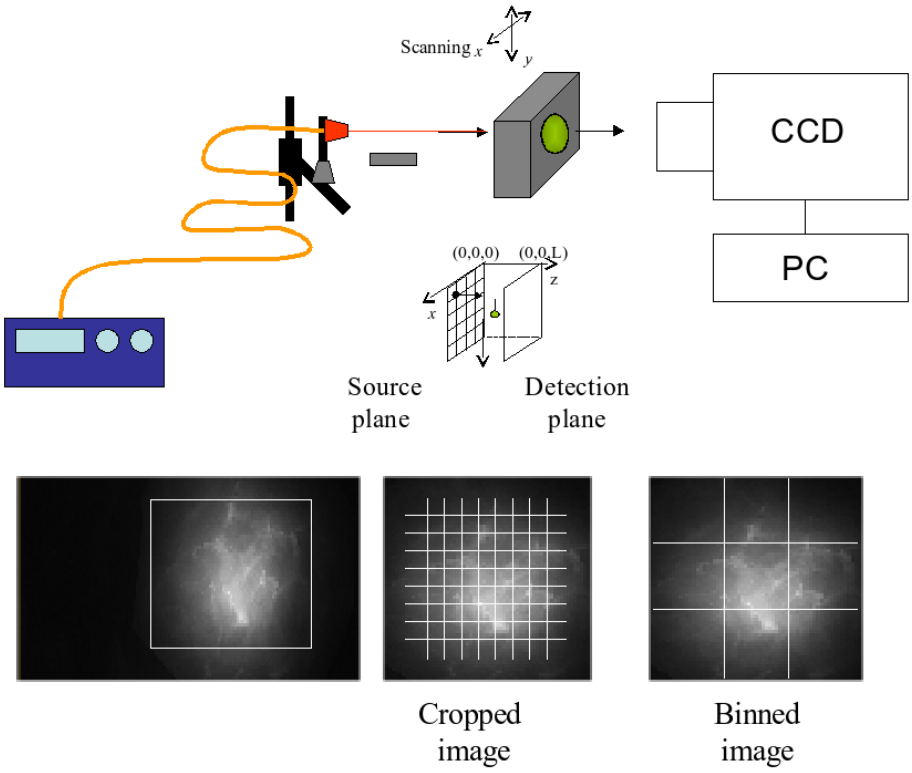

Figure 1. Schematic diagram of the experimental setup.

where the integration is over the $z = z_j$ plane, X_j represents the target, and $\boldsymbol{\rho}_d$ and $\boldsymbol{\rho}_s$ are the lateral coordinates of the detector and the source, respectively. The cross section image of the *j*-th target, X_j, is a 2D map of the absorption/scattering strength of the target. In the Fourier space, the target function X_j can be obtained from Eq. (4) as

$$X_j(\mathbf{q}) = -\frac{\Delta I_j(\mathbf{q}-\mathbf{q}_s, \mathbf{q}_s)}{G(\mathbf{q}-\mathbf{q}_s, z_d, z_j)G^*(\mathbf{q}_s, z_j, z_s)} = -\frac{\Delta I_j(\mathbf{q}, \mathbf{0})}{G(\mathbf{q}, z_d, z_j)G^*(\mathbf{0}, z_j, z_s)}. \tag{5}$$

where $\mathbf{q}$ and $\mathbf{q}_s$ are the spatial frequency on the lateral plane, and "$*$" denotes complex conjugate. We have chosen $\mathbf{q}_s = 0$ in the evaluation of the target function Eq. (5) since sources are usually much sparser than detectors in our setup where a CCD camera is used to detect the light emission at the surface. The inverse Fourier transforms of $X_j(\mathbf{q})$ yields the high resolution cross section image of the *j*-th target due to the high density of detecting cells of the CCD. The size of the target is determined by the full width at half maximum (FWHM) of the cross section image X_j.

3. EXPERIMENT

The experimental arrangement is shown schematically in Fig. 1. The light source was a CW He-Ne laser of wavelength 785nm. The specimen of an *ex vivo* normal female breast tissue was contained in a transparent plastic box. One of the sides of the box could be moved to uniformly compress and hold the tissue specimen in position. The breast tissue specimen consisted primarily of adipose tissue. A small piece of cancerous human breast tissue was placed inside the normal breast tissue specimen at the mid-plane. The breast tissues were provided to us by National Disease Research Interchange under an Internal Review Board approval at the City College of New York. The thickness of the breast tissue specimen was measured to be 33mm when hold in the plastic box with a gentle compression. The sample was scanned 22 by 16 in the x and y direction, respectively, with a step size of 2mm. Images are reconstructed for the volume of $42 \times 30 \times 33\text{mm}^3$.

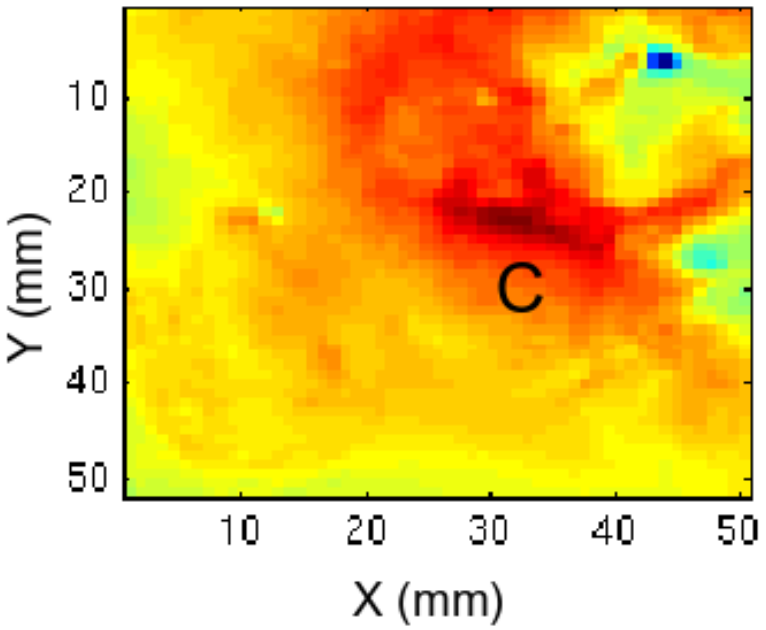

Figure 2. Independent light intensity distributions on the detector plane obtained by OPTICA for the cancer site. The cancer site (C) was found at a depth of $14.8mm$.

4. RESULTS

A typical raw image measured on the detector plane at one scanning position is shown in the inset of Fig. 1. The average of all the 22×16 images was used to obtain the optical property of the background medium. The absorption coefficient of the background medium is found to be $\mu_a = 0.0039\mathrm{mm}^{-1}$ assuming the transport mean free path $l_t = 1\mathrm{mm}$. Each raw image is first cropped to retain the region within the window of $42 \times 30\mathrm{mm}^2$ over which image reconstruction would be performed, and binned to enhance the signal-to-noise ratio. All the binned images corresponding to illumination of the grid points in sequence were then stacked, and used as input for independent component analysis.

The independent light intensity distributions obtained by OPTICA is displayed in Fig. 2. The cancer site was found at the depth of $14.8mm$ from fitting the independent light intensity distribution to the background Green's function.

The back-projection of the detected signal for the cancer site (C) produced its cross section images at the depth of $14.8mm$ in Fig. 3. The corresponding profile along the horizontal direction is displayed on the right for the target. The cancer site is estimated to be $11mm$ in size and it scatters light more strongly. Representative histology of the site is displayed as the inset.

The investigated *ex vivo* breast sample contained minimal amount of blood and hence the reconstructed images is for the scattering property of the sample. The change of μ_s' for the targets can further be estimated from the reconstructed independent component (s_j and a_j) for the site. It was found site C has enhanced scattering compared to the background (mainly adipose tissue). Subsequent pathological analysis confirmed the site C as tumor.

5. DISCUSSION

The nature of the inhomogeneity (either absorptive or scattering or mixed) can be discovered by OPTICA with CW measurement when the signal to noise ratio is high.[6,7] When the signal to noise ratio is not favorable, the recovered independent component will be due to both absorption and scattering perturbations at the site of the inhomogeneity. The strength of the inhomogeneity will be proportional to $\delta\mu_a + \kappa^2\delta D = \delta\mu_a + (\mu_{a_0} - i\omega/c)\delta D/D_0$. This provides a very simple approach to discriminate absorption vs scattering if multiple modulation frequencies ω are available. The capability of OPTICA separating absorption from scattering inhomogeneities can be significantly improved with a time-domain or frequency domain measurement.

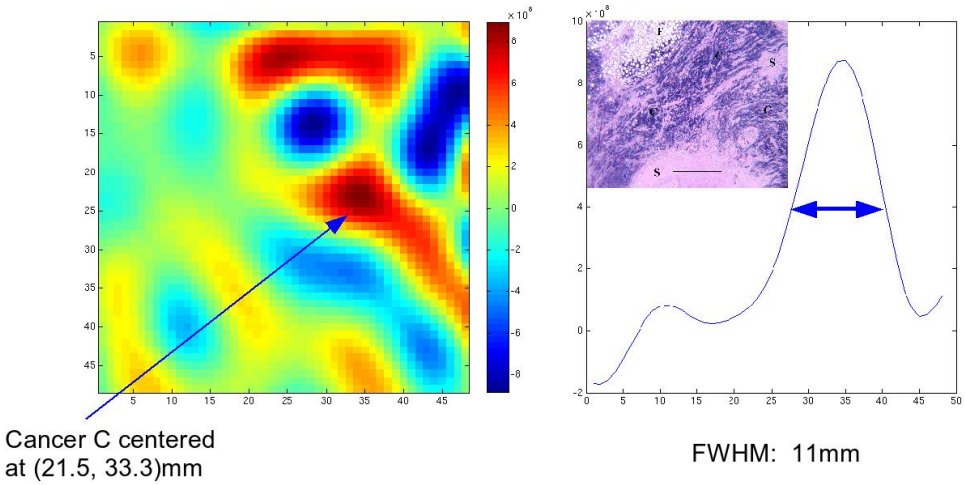

Figure 3. The cross section image for the cancer site at the depth of $14.8mm$. The cancer site is estimated to be $11mm$ in size and scatters light more strongly than the background. The right pane shows the profiles of the target along the horizontal direction. Representative histology of the site is displayed as the inset.

ACKNOWLEDGMENTS

This work is supported in part by US Army Medical Research and Materials Command, ONR, NYSTAR, and CUNY organized research programs. M. X. thanks Fairfield University for startup funds. M. Alrubaiee thanks NSF for an Advance Placement Fellowship. We acknowledge Dr. W. Cai for helpful discussions.

REFERENCES

1. A. P. Gibson, J. C. Hebden, and S. R. Arridge, "Recent advances in diffuse optical imaging," *Phys. Med. Biol.* **50**, pp. R1–R43, 2005.
2. M. A. O'Leary, D. A. Boas, B. Chance, and A. G. Yodh, "Experimental images of heterogeneous turbid media by frequency-domain diffusing-photon tomography," *Opt. Lett.* **20**, pp. 426–428, 1995.
3. M. Xu, M. Lax, and R. R. Alfano, "Time-resolved Fourier optical diffuse tomography," *J. Opt. Soc. Am. A* **18**(7), pp. 1535–1542, 2001.
4. P. M. Morse and H. Feshbach, *Methods of theoretical physics*, vol. I and II, McGraw-Hill, New York, 1953.
5. M. Xu, M. Alrubaiee, S. K. Gayen, and R. R. Alfano, "Three-dimensional localization and optical imaging of objects in turbid media using independent component analysis," *Appl. Opt.* **44**, pp. 1889–1897, 2005.
6. M. Xu, M. Alrubaiee, S. K. Gayen, and R. R. Alfano, "Optical imaging of turbid media using independent component analysis: Theory and simulation," *J. Biomed. Opt.* **10**, p. 051705, 2005.
7. M. Alrubaiee, M. Xu, S. K. Gayen, and R. R. Alfano, "Tomographic imaging of scattering objects in tissue-like turbid media using independent component analysis," *Appl. Phys. Lett.* **87**, p. 191112, 2005.
8. M. Alrubaiee, M. Xu, S. K. Gayen, and R. R. Alfano, "Localization and cross section reconstruction of fluorescent targets in *ex vivo* breast tissue using independent component analysis," *Appl. Phys. Lett.* **89**, p. 133902, 2006.